Electronic Supplementary Material (ESI) for Inorganic Chemistry Frontiers.
This journal is © the Partner Organisations 2023

Electronic supplementary information for

Dy@D_2(21)-C_{84}: Isolation and crystallographic characterization of a rare trivalent C_{84}-based monometallofullerene

Wangqiang Shen,*[a] Lei Lou,[b] Yiao Wei,[c] Lipiao Bao,[c] Guangqing Xu,[a] Peng Jin,*[b] Jun Lv*[a] and Xing Lu*[c]

[a] *School of Materials Science and Engineering, Hefei University of Technology, Hefei 230009, P. R. China*

[b] *School of Materials Science and Engineering, Hebei University of Technology, Tianjin 300130, P. R. China*

[c] *School of Materials Science and Engineering, Huazhong University of Science and Technology, Wuhan 430074, P. R. China*

Table of Contents

References.

Experimental details

General characterizations. High-performance liquid chromatography (HPLC) was conducted on an LC-908 machine (Japan Analytical Industry Co., Ltd.) with toluene as mobile phase. Matrix-assisted laser desorption ionization time of flight (LDI-TOF) mass spectrometry was measured on a BIFLEX III spectrometer (Bruker Daltonics Inc., Germany). Vis-NIR absorption spectra were measured on a PE Lambda 750S spectrophotometer (PerkinElmer, US) in CS_2. Cyclic voltammograms (CV) was measured in o-dichlorobenzene on a CHI-660E workstation, with 0.05 M $TBAPF_6$ as supporting electrolyte. A three-electrode cell consisting of a Pt counter electrode, a glassy carbon working electrode, and a silver reference electrode was used for each CV measurement.

Synthesis and isolation of Dy@*D*₂(21)-C₈₄. Dy@D_2(21)-C_{84} was synthesized in a modified Krätschmer−Huffman fullerene generator by vaporizing composite graphite rods (Φ8 × 100 mm) containing a mixture of Dy_2O_3 and graphite powder (molar ratio of Dy/C = 1:12) with the addition of 300 mbar He gas. After synthesis, the raw soot was collected and extracted by using CS_2, then the solvent was removed by using a rotary evaporator. The solid was redissolved in toluene, the solution was filtered, and then subjected to HPLC separations. The crude extraction was injected into a Buckyprep column with toluene as eluent, fraction F-5 was collected in 55-61 min (**Figure S1**). Subsequently, fraction F-5 was treated with $SnCl_4$ which leaded to the rapid enrichment of $SnCl_4$-EMF complexes as precipitate, which easily decompose to provide pure Dy-containing EMF powders by a simple water treatment [S1,S2]. The powders were dissolved in a CS_2 solution, the solution was dried by a rotary evaporator, and the obtained solid residue was dissolved in toluene and filtered to get the clear solution containing Dy-containing EMF (as shown in **Scheme S1**). F-5p was separated through a two-step HPLC separation with toluene as eluent. The first step was performed on a Buckyprep-M column, and fraction F-5p-3 was collected in 32-35 min (**Figure S2a**). Then, fraction F-5p-3 was reinjected into a Buckyprep column for recycling separation, and F-5p-3-1 (Dy@C_{84}) was collected in 119-137 min (**Figure S2b**).

Single-Crystal XRD measurements of Dy@D_2(21)-C_{84}. Crystalline block of Dy@D_2(21)-C_{84} was obtained by layering a benzene solution of Ni^{II}(OEP) over a CS_2 solution of Dy@C_{84} in a glass tube. Over a 20-day period, the two solutions diffused together, and black crystals formed. Single-crystal

XRD measurement of Dy@D_2(21)-C_{84} was performed at 100 K at BL17B station of Shanghai Synchrotron Radiation Facility. The multi-scan method was used for absorption corrections. The structure was solved by direct method and were refined with SHELXL-2014/7 [S3]. CCDC-2246929 contains the supplementary crystallographic data for this paper. Details of the structural refinement can be found in **Table S2**.

Computational details. Density functional theory calculations were carried out by using the M06-2X[S4] functional in conjunction with the 6-31G* basis set for C[S5] and SDD basis set and corresponding effective core potential for metals[S6] (denoted as 6-31G*~SDD), as implemented in the Gaussian 16 software package[S7].

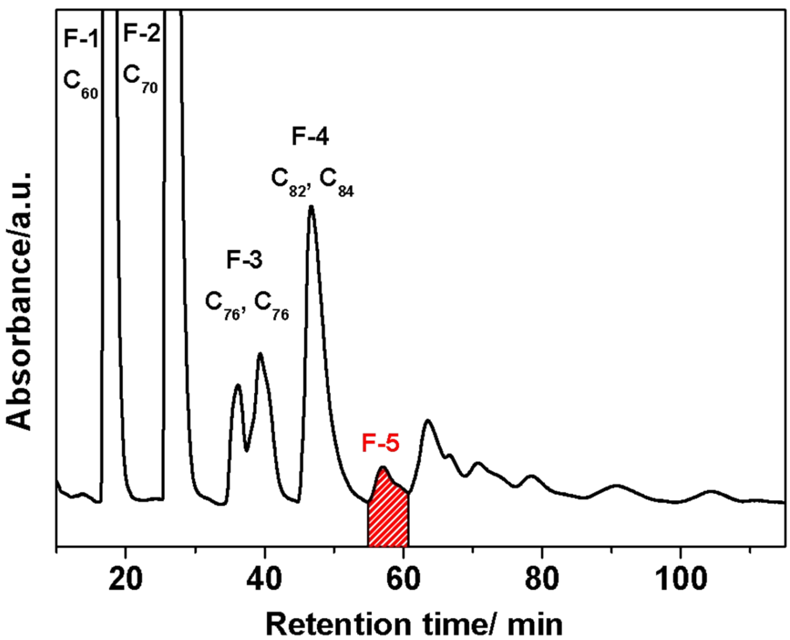

Figure S1. Isolation of raw soot extract on a Buckyprep column. Conditions: Φ = 20 mm × 250 mm, eluent = toluene, flow rate = 9.99 mL/min, detection wavelength = 330 nm, room temperature.

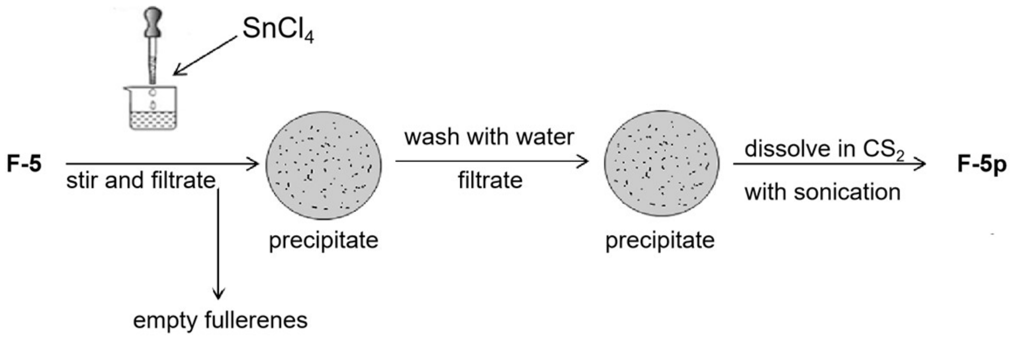

Scheme S1. The process of separation of Dy-EMFs from F-5 with $SnCl_4$.

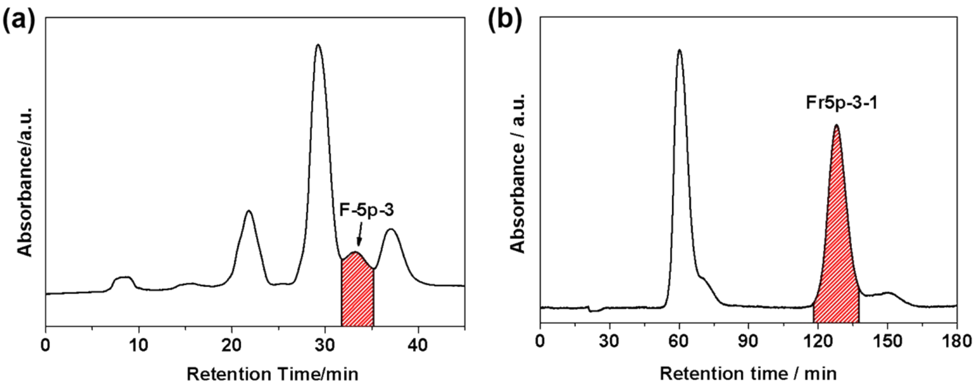

Figure S2. Isolation schemes of Dy@D_2(21)-C_{84}. HPLC chromatograms of (a) F-5p-1 obtained by a Buckyprep-M column and (b) F-5p-3-1(Dy@D_2(21)-C_{84}) obtained by a Buckyprep column. Conditions: Φ = 20 mm × 250 mm, eluent = toluene, flow rate = 9.99 mL/min, detection wavelength = 330 nm, room temperature.

Table S1. Details of the vis-NIR absorptions of Dy@D_2(21)-C_{84}.

Compound	Vis-NIR absorption bands (nm)	Onset (nm)	Optical Bandgap (eV)[a]
Dy@D_2(21)-C_{84}	593, 646, 773, 836, 959	1485	0.84

[a] Optical Bandgap (eV) ≈ 1240/onset (nm).

Table S2. Crystallographic Data of Dy@D_2(21)-C_{84}.

Compound	Dy@D_2(21)-C_{84}•Ni^{II}(OEP)•1.5(C_6H_6)
T, K	100(2)
λ, Å	0.6525
color/habit	black / block
Empirical formula	C258 H106 Dy2 N8 Ni2
fw	3759.86
crystal system	monoclinic
space group	C2/m
a, Å	27.054(1)
b, Å	17.051(6)
c, Å	17.770(6)
α, deg	90.000
β, deg	106.784(1)
γ, deg	90.000
V, Å^3	7848.0(5)
ρ, g/cm^3	1.591
μ, mm^{-1}	0.996
R1 [reflections with I>2σ(I)]	0.1726
wR2 (all data)	0.3735

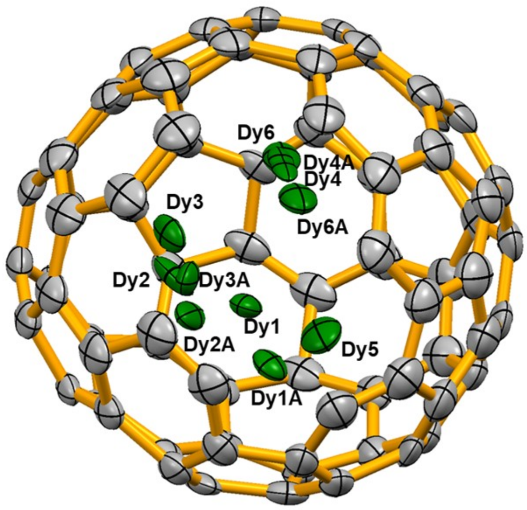

Figure S3. Positions of the disordered dysprosium sites in Dy@D_2(21)-C_{84}. Atoms labeled with an "A" are generated by crystallographic operation.

Table S3. The fractional occupancies of the disordered dysprosium sites in Dy@D_2(21)-C_{84}.

EMFs	Fractional occupancy of the Dy positions					
	Dy1/Dy1A	Dy2/Dy2A	Dy3/Dy3A	Dy4/Dy4A	Dy5	Dy6/Dy6A
Dy@D_2(21)-C_{84}	0.144	0.122	0.085	0.081	0.066	0.035

The atom with a suffix 'A' is generated by crystallographic operation.

Table S4. Relative energies of low-lying Dy@C_{84} isomers with different spin multiplicities (*M*). The ground state for each isomer is highlighted in bold.

isomer	*M*	ΔE(kcal/mol)
Dy@C_2(13)-C_{84}	5	0.8
	7	**0.0**
Dy@D_2(21)-C_{84}	5	53.0
	7	**1.7**
Dy@D_{3d}(19)-C_{84}	5	34.2
	7	**2.4**
Dy@C_1(12)-C_{84}	**5**	**4.0**
	7	4.7
Dy@C_{2v}(17)-C_{84}	**5**	**6.3**
	7	7.9
Dy@C_s(10)-C_{84}	**5**	**8.7**
	7	9.1
Dy@D_2(22)-C_{84}	5	22.5
	7	**9.4**
Dy@C_2(9)-C_{84}	5	9.9
	7	**9.9**
Dy@C_{2v}(7)-C_{84}	5	28.1
	7	**16.1**
Dy@C_2(11)-C_{84}	5	21.6
	7	**16.2**
Dy@D_{2d}(23)-C_{84}	**5**	**16.3**
	7	20.8
Dy@C_2(8)-C_{84}	**5**	**19.2**
	7	19.7
Dy@C_2(15)-C_{84}	**5**	**23.5**
	7	27.5
Dy@C_2(16)-C_{84}	5	69.3
	7	**29.0**

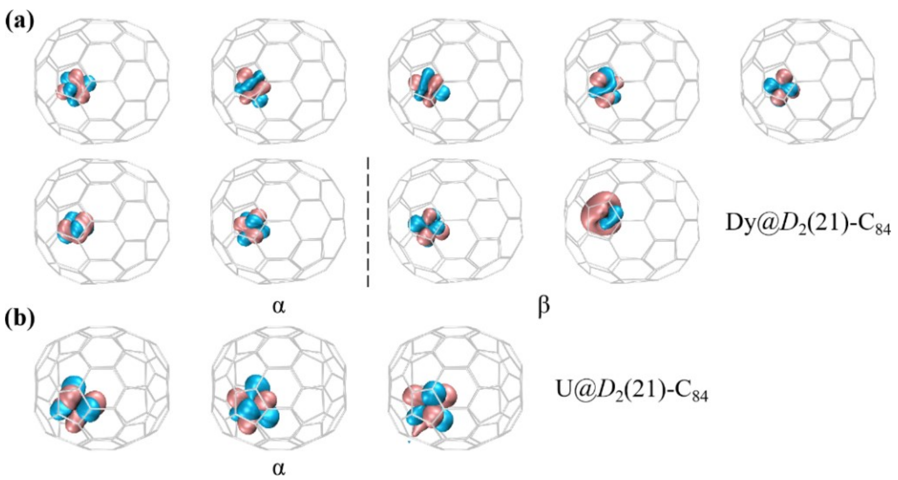

Figure S4. Occupied f-type localized molecular orbitals of (a) Dy@D_2(21)-C_{84} and (b) U@D_2(21)-C_{84}.

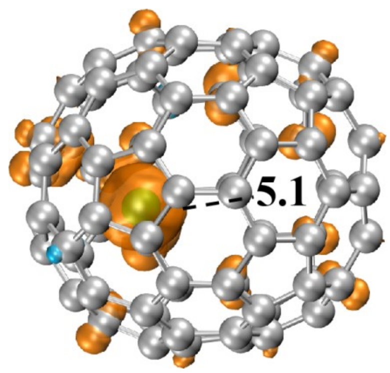

Figure S5. Spin density distribution of Dy@D_2(21)-C_{84} (isovalue: ±0.003 au) with spin population values for the Dy atom.

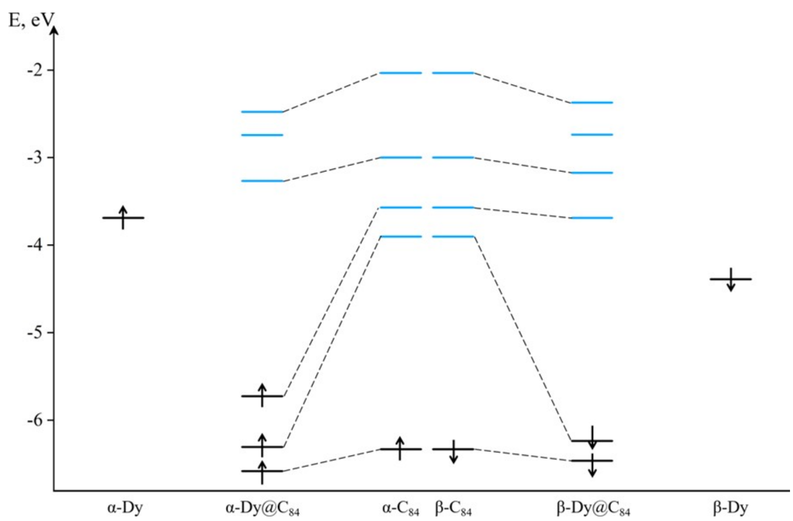

Figure S6. Orbital interaction diagram of Dy@D_2(21)-C_{84}. Occupied and unoccupied orbitals are denoted by black and blue lines, respectively. Three α/β LUMOs of C_{84} contribute to the HOMOs of Dy@D_2(21)-C_{84}, thus confirming the acceptance of three electrons from the Dy atom.

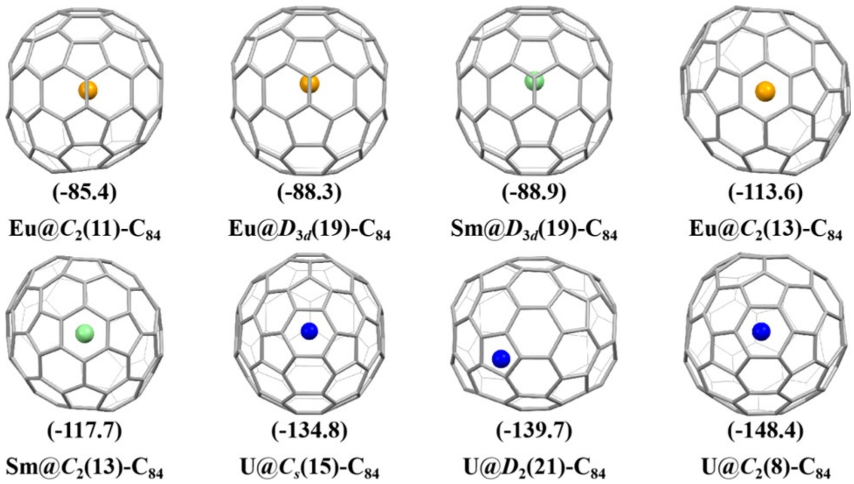

Figure S7. Optimized structures and encapsulation energies (kcal/mol) of M@C_{84}(M = Sm, Eu, U). C: gray, Sm: light green, Eu: orange, U: blue.

Table S5. Relative energies of M@C_{84} with different spin multiplicities (*M*) at the M06-2X/6-31G*~SDD level of theory. The ground state for each molecule is highlighted in bold.

Species	*M*	△E (kcal/mol)
Eu@C_2(11)-C_{84}	6	15.9
	8	**0.0**
	10	16.3
Eu@D_{3d}(19)-C_{84}	6	24.3
	8	**0.0**
	10	18.2
Sm@D_{3d}(19)-C_{84}	5	14.9
	7	**0.0**
	9	15.0
Eu@C_2(13)-C_{84}	6	100.0
	8	**0.0**
	10	29.7
Sm@C_2(13)-C_{84}	5	78.7
	7	**0.0**
	9	33.8
U@C_s(15)-C_{84}	**3**	**0.0**
	5	5.3
U@D_2(21)-C_{84}	3	10.8
	5	**0.0**
U@C_2(8)-C_{84}	**3**	**0.0**
	5	2.1

References

[S1] C. Pan, L. Bao, X. Yu, H. Fang, Y. Xie, T. Akasaka, X. Lu, Facile Access to Y_2C_{2n} (2n = 92–

130) and Crystallographic Characterization of $Y_2C_2@C_1(1660)-C_{108}$: A Giant Nanocapsule with a Linear Carbide Cluster, *ACS Nano.* 2018, **12**, 2065–2069.

[S2] K. Akiyama, T. Hamano, Y. Nakanishi, E. Takeuchi, S. Noda, Z. Wang, S. Kubuki, H. Shinohara, Non-HPLC Rapid Separation of Metallofullerenes and Empty Cages with $TiCl_4$ Lewis Acid, *J. Am. Chem. Soc.* 2012, **134**, 9762–9767.

[S3] G. M. Sheldrick, Crystal Structure Refinement with SHELXL. *Acta Crystallogr. Sect. C Struct. Chem.* 2015, **71**, 3–8.

[S4] Y. Zhao, D. G. Truhlar, The M06 Suite of Density Functionals for Main Group Thermochemistry, Thermochemical Kinetics, Noncovalent Interactions, Excited States, and Transition Elements: Two New Functionals and Systematic Testing of Four M06-Class Functionals and 12 Other Functionals, *Theor. Chem. Acc.* 2008, **120**, 215–241.

[S5] W. J. Hehre, R. Ditchfield, J. A. Pople, Self—Consistent Molecular Orbital Methods. XII. Further Extensions of Gaussian—Type Basis Sets for Use in Molecular Orbital Studies of Organic Molecules. *J. Chem. Phys.* 1972, **56**, 2257–2261.

[S6] X. Cao, M. Dolg, Segmented Contraction Scheme for Small-Core Lanthanide Pseudopotential Basis Sets. *J. Mol. Struct. THEOCHEM.* 2002, **581**, 139–147.

[S7] M. J. Frisch, G. W. Trucks, H. B. Schlegel, G. E. Scuseria, M. A. Robb, J. R. Cheeseman, G. Scalmani, V. Barone, G. A. Petersson and others, Gaussian 16, Revision C.01. Gaussian, Inc., Wallingford CT, 2019.